We are IntechOpen, the world's leading publisher of Open Access books Built by scientists, for scientists

4,800
Open access books available

122,000
International authors and editors

135M
Downloads

Our authors are among the

154
Countries delivered to

TOP 1%
most cited scientists

12.2%
Contributors from top 500 universities

CLARIVATE ANALYTICS BOOK CITATION INDEX INDEXED

WEB OF SCIENCE™

Selection of our books indexed in the Book Citation Index in Web of Science™ Core Collection (BKCI)

Interested in publishing with us?
Contact book.department@intechopen.com

Numbers displayed above are based on latest data collected.
For more information visit www.intechopen.com

8

Chemical Indices of the Biomimetic Models of Oxyhemocyanin and Oxytyrosinase

Yu Takano[1], Kizashi Yamaguchi[2] and Haruki Nakamura[1]
[1]*Institute for Protein Research, Osaka University*
[2]*Graduate School of Science, Osaka University*
Japan

1. Introduction

The $Cu_2(\mu\text{-}\eta^2\text{:}\eta^2\text{-}O_2)$ species has attracted attention in the model studies of type III copper proteins because this structure is suggested as an important motif in biological systems (Karlin and Tyeklár, 1993; Kitajima and Moro-oka, 1994). Although oxyhemocyanin (oxyHc) and oxytyrosinase (oxyTy) have this species in the active site, they show different functions: oxygen transport and oxygen activation, respectively (Cooksey et al., 1997; Cuff et al., 1998; Holm et al., 1996; Solomon et al., 1992).

Synthetic modeling approaches have greatly developed our understanding of the chemical characters of the $Cu_2(\mu\text{-}\eta^2\text{:}\eta^2\text{-}O_2)$ species (Cahoy et al., 1999; Funahashi et al., 2008; Hu et al., 2001; Kitajima et al., 1992; Kitajima et al., 1989; Kodera et al., 2004; Kodera et al., 1999; Lam et al., 2000). Kitajima et al. succeeded in synthesizing $[(HB(3,5\text{-}iPr_2\text{-}Pz)_3)Cu]_2(O_2)$ ($HB(3,5\text{-}iPr_2\text{-}Pz)_3$ = hydrotris{3,5-diisopropyl-pyrazolyl}borate (Trofimenko, 1999)) (**1**), which showed remarkable physicochemical similarities to oxyHc and oxyTy, and determining the crystal structures of the complex, which first characterized a $Cu_2(\mu\text{-}\eta^2\text{:}\eta^2\text{-}O_2)$ structure for the active site of oxyHc, before the X-ray crystallographic studies of Hc were reported (Kitajima et al., 1989). Tolman and his collaborators synthesized $[(iPr_3TACD)Cu]_2(\mu\text{-}\eta_2\text{:}\eta_2\text{-}O_2)$ (iPr_3TACD = 1,5,9-triisopropyl-1,5,9-triazacyclodecane (**2**) to understand how the nature of the tridendate macrocyclic supporting ligand influences the relative stability of the isomeric $\mu\text{-}\eta^2\text{:}\eta^2$-peroxo- and bis(μ-oxo)dicopper complexes (Lam et al., 2000). They showed that low-temperature oxygenation of $[(iPr_3TACD)Cu]_2(CH_3CN)]SbF_6$ yielded a $\mu\text{-}\eta^2\text{:}\eta^2$ product with no trace of the bis(μ-oxo) isomer and concluded that the size of the ligand substituents and the ligand macrocycle ring size are key factors in controlling the relative stabilities of the $\mu\text{-}\eta_2\text{:}\eta_2\text{-}O_2$-peroxo and bis(μ-oxo) forms. Kodera et al. reported the reversible dioxygen binding by the room-temperature-stable complex, $[(L1)Cu]_2(\mu\text{-}\eta_2\text{:}\eta_2\text{-}O_2)$ (L1 = 1,2-bis[2-(1,1-bis(6-methyl-2-pyridyl)ethyl)-6-pyridyl]ethane) (**3**), and showed that the long Cu–O bonds and the strong O–O bond of **3** are favorable for easy release of O_2 since the O–O stretch of **3** is the strongest for $Cu_2(\mu\text{-}\eta^2\text{:}\eta^2\text{-}O_2)$ complexes including oxyHc from the resonance Raman spectrum (Kodera et al., 2004). Masuda and his coworkers synthesized a new $Cu_2(\mu\text{-}\eta_2\text{:}\eta_2\text{-}O_2)$ complex formed with α-isosparteine and benzoate (**4**) and determined the novel coordination structure of a carboxylate-bridged butterfly type $\mu\text{-}\eta^2\text{:}\eta^2$-peroxide dicopper core (Funahashi et al., 2008). It was shown that the butterfly core is supported by

benzoate in the axial position, losing its planarity despite the Jahn–Teller effect on the Cu(II) d^9-configuration. Fig. 1 illustrates the coordinating ligands to the $Cu_2(\mu\text{-}\eta^2\text{:}\eta^2\text{-}O_2)$ core of the biomimetic models **1–4**, and Fig. 2 shows the X-ray crystallographic structures of **1–4**.

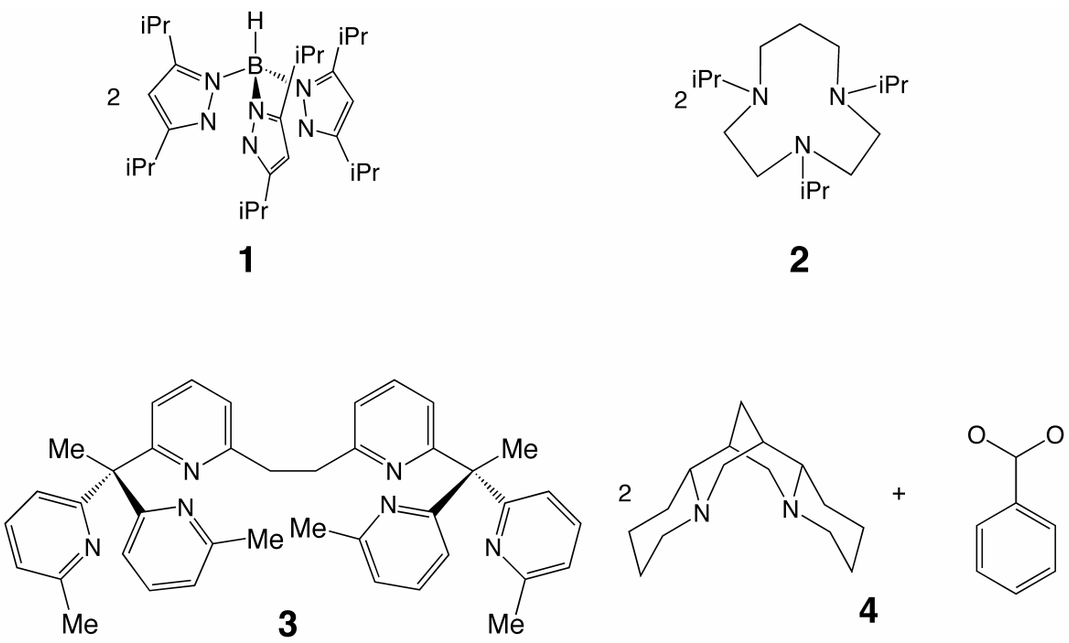

Fig. 1. Coordinating ligands utilized for the biomimetic model of Hc **1–4**.

Several theoretical investigations have also been performed on models of the dicopper active site (Aullón et al., 2006; Benson et al., 2002; Cramer et al., 2003; Cramer and Pak, 2001; Gresh et al., 2002; Siegbahn, 2006; Siegbahn and Wirstam, 2001). Siegbahn studied the catalytic mechanisms of tyrosinase and catechol oxidase using Cu_2O_2 complex coordinated by six imidazole ligands at the UB3LYP level of theory (Siegbahn, 2006; Siegbahn and Wirstam, 2001). Cramer et al. investigated the mechanism of the intramolecular C-H bond cleavage in $[LCu]_2(\mu\text{-}O)_2$ (L = 1,4,7-tribenzyl-1,4,7-triazacyclononane) (Cramer et al., 2003; Cramer and Pak, 2001) using the integrated molecular orbital molecular mechanics (Maseras and Morokuma, 1995) with DFT and universal force field (Rappe et al., 1992). Aullón et al. performed UB3LYP calculations on binuclear $[(Tp)Cu]_2(\mu\text{-}O)_2$ complexes (Tp = tris(pyrazolyl)borate) to examine the effect of the substituents of the Tp ligands on dioxygen activation and stabilization (Aullón et al., 2006).

Previously, we investigated the magnetic couplings and the potential energy surface for the reversible binding process of the model of Hc using unrestricted Hartree–Fock and spin-polarized density functional theory (DFT) (Becke's half and half LYP (UBHandHLYP), UB3LYP, and UBLYP) (Takano et al., 2009; Takano et al., 2001; Takano and Yamaguchi, 2007). In this model, each Cu ion is coordinated by three methylimidazole. We concluded that the superexchange interaction via the bridging dioxygen causes a strong antiferromagnetic couplings between the two copper ions of the model of oxyHc and that the structural conversion from oxy to deoxyHc controls the reversible binding of dioxygen for Hc.

To comprehend the chemical character of the $Cu_2(\mu\text{-}\eta^2\text{:}\eta^2\text{-}O_2)$ complexes, we have investigated the magnetic interaction and the nature of the chemical bond of the biomimetic

models of oxyHc and oxyTy, **1–4**, from the viewpoint of the shape and symmetry of the natural orbitals and chemical indices. We compared the geometries, magnetic couplings, and nature of chemical bonds of the optimized structures to those of the X-ray structures.

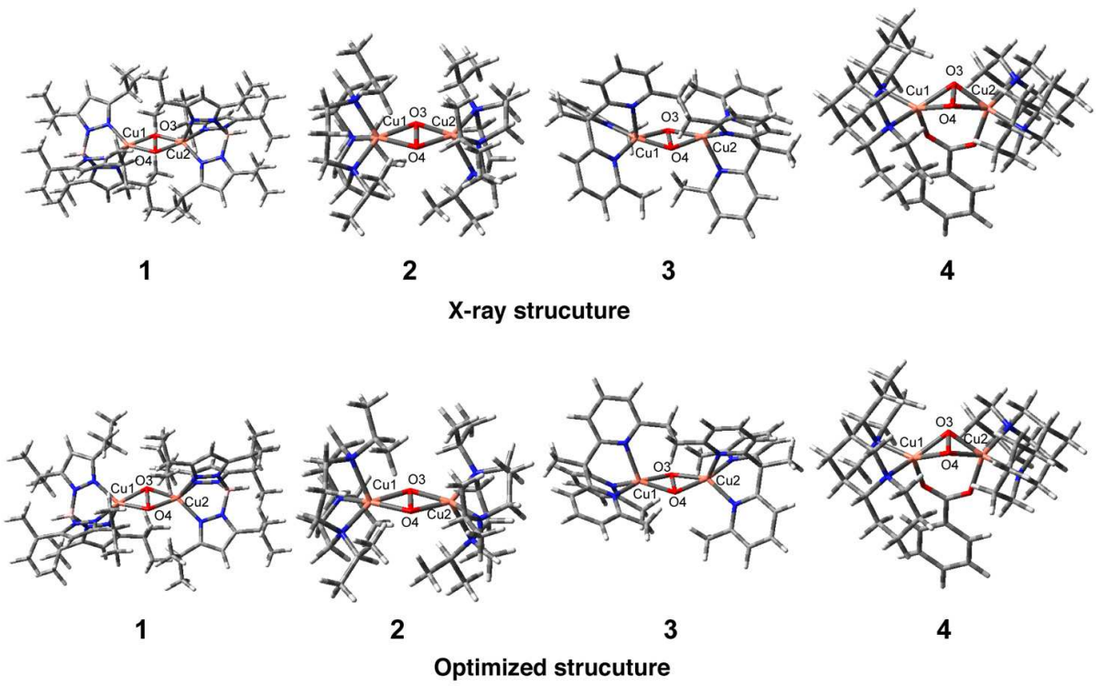

Fig. 2. X-ray crystallographic structures and optimized structures of **1–4**. Site numbers Cu1, Cu2, O3, and O4 are also illustrated.

2. Theoretical background

2.1 Magnetic coupling constant (J_{ab})

Since a large number of transition metal complexes have unpaired d electrons, magnetic properties of transition metal complexes have been investigated in order to understand the molecular structures and the electronic structures. Magnetic coupling constants (J_{ab}) can be experimentally determined by the measurement of magnetic susceptibility. Recent development of computational techniques of quantum chemistry has made theoretical calculations of J_{ab} values possible (Takano et al., 2001). Let us consider the superexchange interactions between Cu(II)L_3 (L: ligand) fragments via peroxide. Cupric ion, Cu(II), has the d^9 configuration with half spin ($S = 1/2$). If each spin is mainly localized on one site (a or b site), as illustrated in **I** of Fig. 3, we can estimate J_{ab} values between magnetic sites on the basis of the Heisenberg model (Onishi et al., 2001; Salem, 1982; Soda et al., 2000; Takano et al., 2008; Takano et al., 2002a; Takano et al., 2001; Takano et al., 2000; Takano and Yamaguchi, 2007) using the energy gap by spin-polarized DFT calculations between the highest spin (HS) and lowest spin (LS) states,

$$H = -2\sum J_{ab}\mathbf{S}_a \bullet \mathbf{S}_b, \tag{1}$$

where $\mathbf{S_a}$ and $\mathbf{S_b}$ represent the spins at sites a and b, respectively. However, spin-polarized DFT solutions in the LS states usually exhibit the broken symmetry problem (Isobe et al.,

2002; Mitani et al., 2000a; Onishi et al., 2001; Salem, 1982; Takano et al., 2008; Takano et al., 2002a; Takano et al., 2001; Takano et al., 2000; Takano and Yamaguchi, 2007). Spin projection of the broken symmetry solutions should be carried out to eliminate the spin contaminations.

$$J_{ab} = \frac{^{LS}E_X - ^{HS}E_X}{^{HS}\langle S^2 \rangle_X - ^{LS}\langle S^2 \rangle_X}, \tag{2}$$

where ${}^{Y}E_X$ and ${}^{Y}\langle S^2 \rangle_X$ denote the total energy and total angular momentum of the spin state Y by spin-polarized DFT, respectively.

2.2 Natural orbitals

The molecular orbital picture is also feasible for elucidation of the origin of the magnetic interaction between the Cu(II) ions. In order to obtain molecular orbital-theoretical explanation of the magnetic interactions, the natural orbitals of the spin-polarized DFT solutions were determined by diagonalizing their first-order density matrices (Onishi et al., 2001; Salem, 1982; Takano et al., 2008; Takano et al., 2002a; Takano et al., 2001; Takano et al., 2000; Takano and Yamaguchi, 2007) as

$$\rho(\mathbf{r},\mathbf{r}') = \sum n_i \phi_i^*(\mathbf{r}) \phi_i(\mathbf{r}') \tag{3}$$

where n_i denotes the occupation number of the natural orbital ϕ_i. The occupation numbers of the bonding and anti-bonding natural orbitals were almost 2.0 and 0.0, respectively, except for the two singly occupied natural orbitals (SONOs), for which the occupation numbers were close to 1.0. The broken symmetry bonding orbitals are generally given by the in- and out-of phase combinations of the bonding (ϕ) and antibonding (ϕ^*) DFT natural orbital

$$\psi_i^{\pm} \cong (\cos\omega)\phi_i \pm (\sin\omega)\phi_i^* \tag{4}$$

where ω is the orbital mixing coefficient (Onishi et al., 2001; Salem, 1982; Takano et al., 2008; Takano et al., 2002a; Takano et al., 2001; Takano et al., 2000; Takano and Yamaguchi, 2007).

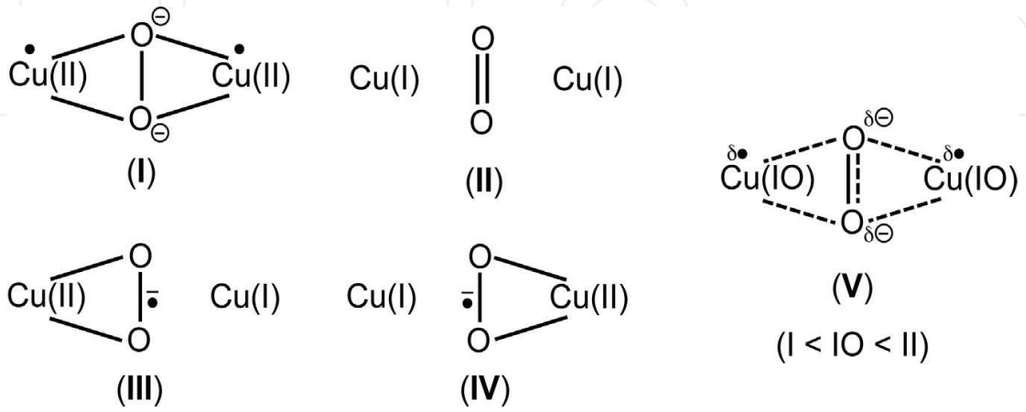

Fig. 3. Valence bond description of the Cu_2O_2 bond.

The orbital overlap $T_i = \left\langle \psi_i^+ \middle| \psi_i^- \right\rangle$ between magnetic orbitals is a measure of the SE interaction, namely T_i = 0 for pure metal diradical and T_i = 1 for the closed-shell pair. The occupation numbers of the bonding and antibonding DNO are expressed by the T_i value;

$$n_i = 1 + T_i, \quad n_i^* = 1 - T_i \tag{5}$$

The total spin angular momentum for the BS solution is given by

$$^{LS}\langle S^2 \rangle = S_{min}(S_{min}+1) + \Sigma\,(1 - T_i^2) \tag{6}$$

2.3 Chemical indices

In theoretical and coordination chemistries, an important issue is to understand the nature of the chemical bonds in transition metal complexes. Chemical indices are useful criteria for the nature of chemical bonds. Since the broken symmetry solutions are employed in this study, several chemical indices, which are equally defined by the symmetry-adapted CASCI and CASSCF, are expressed in terms of the occupation numbers of DFT natural orbital (Isobe et al., 2003; Mitani et al., 2000a; Yamaguchi, 1990). These indices are used as common criteria for the nature of the chemical bonds of the $Cu_2(\mu\text{-}\eta^2\text{:}\eta^2\text{-}O_2)$ core.

The effective bond order (Isobe et al., 2003; Yamaguchi, 1990) is defined by

$$b_i = \frac{n_i - n_i^*}{2} \tag{7}$$

The effective bond order is a measure of the superexchange interaction; that is, b_i = 0 for pure metal diradical and b_i = 1 for the closed-shell pair.

Classical and quantum information theories and generalized entropies are now well-defined in several different fields to extract information. In chemistry, information entropy (I) is employed to express the characteristic of chemical bonds (Ramirez et al., 1997). The Jaynes information entropy is defined by the occupation number of SONOs to express electron correlation

$$I = -n_i \ln n_i \tag{8}$$

The Jaynes information entropy for the spin-restricted DFT solution of closed-shell systems is given by

$$I_C = -2\ln 2 \tag{9}$$

Then, the normalized Jaynes information entropy is defined as a measure of correlation correction as

$$I_n = \frac{I_C - I}{I_C} \quad \left(0 \le I_n \le 1\right) \tag{10}$$

The I_n value increases with the decrease of T_i in this definition, and it is parallel to the decrease of the effective bond order $\Delta b = 1 - b = 1 - T$ (Isobe et al., 2002). The I_n and Δb values are, therefore, responsible for loss of bond information or covalent bonding.

The unpaired electron density U is defined as the deviation of the post HF and CI wavefunctions from the single Slater determinant (Takatsuka et al., 1978), and it is also expressed by the occupation number as

$$U = n_i\left(2 - n_i\right) \tag{11}$$

Very recently, the U-value is utilized as a measure of electron correlation by Staroverov and Davidson (Staroverov and Davidson, 2000).
The CASCI and CASSCF methods (Roos et al., 1982) are well-accepted approaches to open-shell species. Therefore, it is desirable to clarify mutual relations between the CI and BS methods. The diradical character (Y) is defined by the weight of doubly excited configuration (W_D) involved in the projected BS solution in comparison with CASCI and CASSCF (Isobe et al., 2002; Mitani et al., 2000b) as

$$Y = 2W_{\mathrm{D}} = 1 - \frac{2T_i}{1+T_i^2} = \frac{n_i^2 - 4n_i + 4}{n_i^2 - 2n_i + 2} \tag{12}$$

Thus, all the chemical indices introduced here are related each other through the occupation numbers of natural orbitals, which can be calculated by both symmetry-adapted solutions such as CASSCF and broken-symmetry solutions. These indices are used as common criterion for chemical bonds of biomimetic complexes **1–4**.

3. Computational details

3.1 Computational procedure

All quantum chemical calculations were carried out on the synthetic Cu_2O_2 complexes **1–4** with Gaussian03 program (Frisch et al., 2003).
In DFT calculations, exchange-correlation potentials are generally defined by

$$E_{\mathrm{XC}} = C_1 E_{\mathrm{X}}^{\mathrm{HF}} + C_2 E_{\mathrm{X}}^{\mathrm{Slater}} + C_3 \Delta E_{\mathrm{X}}^{\mathrm{Becke88}} + C_4 E_{\mathrm{C}}^{\mathrm{VWN}} + C_5 \Delta E_{\mathrm{C}}^{\mathrm{LYP}} \tag{13}$$

where $E_{\mathrm{X}}^{\mathrm{HF}}$ is the Hartree–Fock exchange, $E_{\mathrm{X}}^{\mathrm{Slater}}$ is the Slater exchange, $\Delta E_{\mathrm{X}}^{\mathrm{Becke88}}$ is the gradient part of the exchange functional of Becke (Becke, 1988), $E_{\mathrm{C}}^{\mathrm{VWN}}$ is the correlation functional of Vosko, Wilk, and Nusair (Vosko et al., 1980), and $\Delta E_{\mathrm{C}}^{\mathrm{LYP}}$ is the correlation functional of Lee, Yang, and Parr (Lee et al., 1988) which includes the gradient of the density. Parameters, C_i (i = 1–5), are the mixing coefficients. The parameter sets (C_1, C_2, C_3, C_4, and C_5) are taken as (0.00, 1.00, 1.00, 1.00, and 1.00) for BLYP, (0.20, 0.80, 0.72, 1.00, and 0.81) for B3LYP (Becke, 1993), and (0.50, 0.50, 0.50, 1.00, and 1.00) for BHandHLYP (Becke, 1993). Since we showed that UBHandHLYP (referred to as UB2LYP in the previous papers (Takano et al., 2001; Takano and Yamaguchi, 2007)) can be regarded as a reliable method to examine the magnetic couplings and the dioxygen binding process of Hc and the nature of chemical bonds of the biomimetic complexes in the previous papers (Takano et al., 2009; Takano et al., 2001; Takano and Yamaguchi, 2007), we used the UBHandHLYP exchange-correlation functionals to investigate the magnetic couplings and the chemical indices: it is noteworthy that UBHandHLYP is much more reliable than conventional UB3LYP for strongly correlated electron systems such as CuO plane in oxide superconductors (Onishi et al., 2001).

Basis sets employed in all the calculations were Tatewaki–Huzinaga MIDI (533(21)/53(21)/(41)) (Tatewaki and Huzinaga, 1979) plus Hay's d diffuse function (α = 0.1491) (Hay, 1977) for Cu(II) ions, Pople's 6-31G(d) (Hariharan and Pople, 1973) for C, O, N, and B atoms, and 6-31G (Hehre et al., 1972) for H atoms.

3.2 Geometrical parameters for 1–4

The geometrical parameters of **1–4** were taken from the X-ray crystallographic data of Cambridge Structural Database (Allen, 2002) as shown in Fig. 2 (Refcode for **1**: KECZEX, Refcode for **2**: NAPGEQ, Refcode for **3**: BEMNIR, and Refcode for **4**: QOSRAS). Full geometry optimizations of **1–4** were also performed in highest- and lowest-spin states in the gas phase by using the UBHandHLYP functionals with the basis sets mentioned above. The optimized structures were characterized by using harmonic frequency calculations.

4. Comparison between X-ray structures and optimized structures

The geometrical parameters of the X-ray and optimized structures for **1–4** in the most stable state are listed in Table 1. In the geometry optimizations, models **1–3** preferred the lowest spin state to the highest spin state, while model **4** favored the highest spin state over the lowest spin state. The differences between the X-ray and optimized bond distances were within 0.1 Å except for the Cu1–Cu2 , O3–O4, and Cu2–O3 parts of **2** (0.11, 0.11, and 0.15 Å, respectively) and the Cu–N part of **3** (0.12 Å). In the optimization, the changes of the dihedral angles of the Cu_2O_2 core were less than 10˚ except for the d(O3-O4-Cu1-Cu2) and d(Cu1-O3-O4-Cu2) of **1** (21.3˚ and –17.4˚) and d(Cu1-O3-O4-Cu2) of **4** (–10.3˚). These differences between the optimized geometries and the X-ray structures would be due to the effects of crystal packing and the spin contamination errors during the optimization as shown below.

	1		**2**		**3**		**4**	
	X-ray[a]	Opt[b]	X-ray[a]	Opt[b]	X-ray[a]	Opt[b]	X-ray[a]	Opt[b,c]
Cu1-Cu2[d]	3.56	3.58	3.52	3.63	3.52	3.61	3.27	3.24
O3-O4[d]	1.41	1.48	1.37	1.48	1.49	1.47	1.46	1.46
Cu1-O3[d]	1.90	1.95	1.96	1.96	1.92	1.93	1.98	2.08
Cu1-O4[d]	1.93	1.96	1.92	1.97	1.91	2.00	1.87	1.92
Cu2-O3[d]	1.93	1.94	1.81	1.96	1.96	1.98	1.91	1.92
Cu2-O4[d]	1.90	1.98	1.89	1.96	1.90	1.94	1.98	2.05
Cu-N(O)[d,e]	2.08	2.11	2.11	2.17	2.05	2.17	2.03	2.09
d(O3-O4-Cu1-Cu2)[f]	0.0	21.3	10.37	5.30	–15.8	–19.6	48.2	53.7
d(Cu1-O3-O4-Cu2)[f]	180.0	162.6	171.9	176.0	–168.2	–164.7	132.3	122.0

[a] The parameters are taken from the X-ray structures. [b] The parameters were fully optimized at the UBHandHLYP level of theory. [c] Geometry optimization was performed in the highest spin state. [d] Distances are given in angstroms. [e] Average value for bond distances between Cu ion and N or O atom coordinating to $Cu_2(\mu\text{-}\eta^2\text{:}\eta^2\text{-}O_2)$ core. [f] Dihedral angles are given in degrees.

Table 1. Selected Geometrical Parameters for **1–4** in the most stable state at the UBHandHLYP level of theory.

In the biomimetic model **1**, the large changes of the dihedral angles mean that the structure of the Cu_2O_2 core converts from the planar structure to the butterfly one in the geometry optimization. The geometry optimization of **2** kept the core structure planar but expanded the Cu_2O_2 core, indicating that the coordinating ligand of **2** weakly suppresses the Cu_2O_2 core compared to the other ligands. As opposed to **1**, though the dihedral angles of the Cu_2O_2 core of **3** hardly changed in the optimization, the Cu1–Cu2 distance elongated to 0.09 Å, the O3-O4 length slightly shrank, the mean bond distance between the coordinating ligands and the Cu_2O_2 core increased to 0.12 Å. These results imply easy release of oxygen molecule from **3**. The core structure of **4** is the most distorted of all the models **1–4**. Optimization made the Cu_2O_2 core of **4** to be distorted more. It causes the strongly mixing of the character of triplet oxygen molecule, resulting in the stabilization of the highest spin state more than the lowest spin state because triplet oxygen molecule is much more stable than singlet oxygen molecule.

5. Magnetic couplings of the biomimetic model complexes 1-4

5.1 Magnetic coupling constants (J_{ab})

Table 2 summarizes the J_{ab} values for **1–4**. All J_{ab} values calculated with the X-ray structures show strong antiferromagnetic couplings between the Cu(II) ions. The absolute values of the J_{ab} are in the order $|J_{ab}(\mathbf{2})| >> |J_{ab}(\mathbf{1})| > |J_{ab}(\mathbf{3})| >> |J_{ab}(\mathbf{4})|$. This result is mainly brought from the distortion of the Cu_2O_2 core structure because the discrepancies from the planar structure (d(O3-O4-Cu1-Cu2) = 0° and d(Cu1-O3-O4-Cu2) = 180°) for the Cu_2O_2 core of **1–4** are in the order: **1** ≈ **2** < **3** << **4**. The J_{ab} values are sensitive to the change of the Cu_2O_2 structure because the Cu_2O_2 core lies in the labile bonding region (Takano and Yamaguchi, 2007), and the core structure strongly affects the strength of the symmetry-allowed orbital interactions between the symmetric (S) d_{xy}–d_{xy} orbital of the dicopper site and the σ* and π_v* orbitals of O_2 and between the antisymmetric (A) d_{xy}+d_{xy} orbital and the π_h* orbital, as shown in Fig. 4.

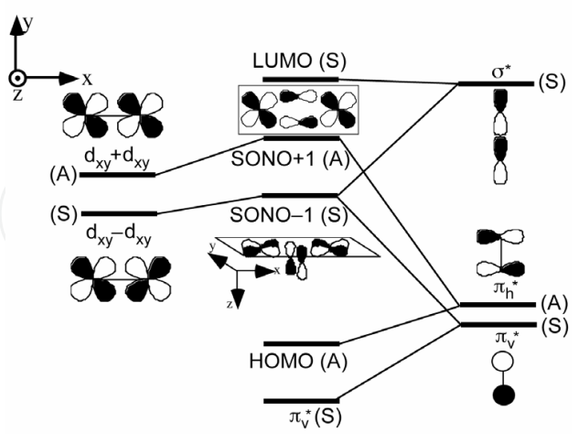

Fig. 4. Orbital diagram of the Cu_2O_2 bond.

The magnetic couplings weakened after full geometry optimization, and, in particular, the J_{ab} value for **4** became positive, indicating a ferromagnetic coupling. This is because of the elongation of the Cu–O–Cu lengths (Cu1–O3 + Cu2–O3 and Cu1–O4 + Cu2–O4) and the change of the dihedral angles. Geometry optimization of **1** remarkably changed the Cu_2O_2

structure from the planar form to the butterfly form. The structural conversion affects the orbital interactions between the Cu(II) ions via peroxide, leading to drastic reduction of the J_{ab} values in magnitude. The larger elongation of the Cu–O–Cu lengths in **2** (0.15 Å for Cu1–O3–Cu2 and 0.12 Å for Cu1–O4–Cu2) and **3** (0.13 Å for Cu1–O4–Cu2) made the magnetic coupling weak, though the shape of the Cu_2O_2 core kept almost planar during geometry optimization. During geometry optimization of **4**, the Cu–O bond lengths elongated by about 0.1 Å, showing that the dioxygen part tends to dissociate from the dicopper core and that the spin crossover from the lowest spin state to the highest spin state occurs (Takano and Yamaguchi, 2007). However, this spin crossover during geometry optimization might be attributed to the spin contamination error (Kitagawa et al., 2007; Saito et al., 2010; Saito et al., 2008). These indicate that the ligands that can hold the Cu_2O_2 core planar lead to the strong antiferromagnetic complexes.

Model	J_{ab}[a]	
	X-ray[b]	Opt[c]
1	–1902	–678.1
2	–1967	–1363
3	–1508	–1020
4	–247.5	35.17

[a] J_{ab} is shown in cm^{-1}. [b] The parameters are taken from the X-ray structures. [c] The parameters were fully optimized at the UBHandHLYP level of theory.

Table 2. Magnetic Coupling constants (J_{ab})[a] Calculated for **1–4** at the UBHandHLYP level of theory.

5.2 Charge and spin density distributions

We have investigated the charge and spin density distributions for **1–4** to understand the characteristics of the magnetic couplings. As listed in Table 3, the charge density on the O–O group varies from the formal charge (–2.0) in **I** to 0.0 in the valence bond configuration **II** in Fig. 3, indicating the back charge transfer from peroxide to cupric ions. The back charge transfer implies that the superexchange interactions are responsible for the strong antiferromagnetic coupling of the biomimetic models.

In Table 3, the spin densities on Cu(II) ions were about 0.7 for **1–4**. The spin density populations indicate the resonance state between the one-electron transfer valence bond configurations **III** and **IV** in Fig. 3. The spin densities on the O–O group are cancelled out in this resonance state **V**; that is, intermediate valence state.

The broken symmetry orbitals in Eq. (4) are approximately expressed by the fragment orbitals responsible for these valence bond configurations in Fig. 3.

$$\psi^{+} \cong \left(\cos\theta\right)\pi_{\mathrm{h}}^{*} + \left(\sin\theta\right)d_{\mathrm{xy}}^{\mathrm{Cu2}} \tag{14}$$

$$\psi^{-} \cong \left(\cos\theta\right)\pi_{\mathrm{h}}^{*} + \left(\sin\theta\right)d_{\mathrm{xy}}^{\mathrm{Cu1}} \tag{15}$$

where θ is the orbital mixing parameter and $d_{\mathrm{xy}}^{\mathrm{Cu1}}$ or $d_{\mathrm{xy}}^{\mathrm{Cu2}}$ denote the localized d_{xy} orbital at Cu1 or Cu2, respectively. The broken symmetry solution is approximately given by $\left|\psi^{+}\overline{\psi}^{-}d_{\mathrm{xy}}^{\mathrm{Cu1}}\overline{d}_{\mathrm{xy}}^{\mathrm{Cu2}}\right|$. The spin density at Cu1 is calculated by

Model			Cu1[a]	Cu2[a]	O3[a]	O4[a]
1	X-ray	Charge	1.082	1.082	–0.594	–0.594
		Spin	0.709	–0.708	0.006	–0.007
	Opt	Charge	1.023	1.075	–0.591	–0.572
		Spin	0.726	–0.727	0.000	–0.000
2	X-ray	Charge	0.985	1.044	–0.641	–0.612
		Spin	0.661	–0.651	–0.009	–0.008
	Opt	Charge	0.929	0.937	–0.604	–0.601
		Spin	0.689	–0.676	–0002	–0.005
3	X-ray	Charge	1.127	1.107	–0.594	–0.611
		Spin	0.701	–0.713	0.022	–0.013
	Opt	Charge	1.071	1.063	–0.610	–0.586
		Spin	0.715	–0.712	0.025	–0.029
4	X-ray	Charge	0.873	0.887	–0.584	–0.601
		Spin	0.688	–0.687	–0.034	0.030
	Opt (HS)[b]	Charge	0.841	0.841	–0.545	–0.545
		Spin	0.666	0.667	0.215	0.215

[a] The site numbers are shown in Fig. 2. [b] Geometry optimization was performed in the highest spin state.

Table 3. Charge and Spin Densities of **1–4** at the UBHandHLYP level of theory.

$$Q_{\mathrm{Cu1}} = \left(1 - \sin^2\theta\right) \cong 0.7 \tag{16}$$

The θ-parameter was determined to be 0.58 rad. The broken symmetry solution after spin projection, namely the resonance state **V**, is obtained by

$${}^1\Phi \cong \left(spin-projected\right)\left|\psi^+\overline{\psi}^- d_{\mathrm{xy}}^{\mathrm{Cu1}}\overline{d}_{\mathrm{xy}}^{\mathrm{Cu2}}\right| = N\left(\sum C_{\mathrm{X}}\,{}^1\Phi_{\mathrm{VB}}(\mathrm{X})\right) \tag{17}$$

where ${}^1\Phi_{\mathrm{VB}}(\mathrm{X})$ denotes the pure singlet valence bond wavefunction responsible for the valence bond structure X (= **I–IV**), and N is the normalizing factor. The configuration mixing parameters C_{X} are defined by the orbital mixing parameter ω.

$$C_{\mathrm{I}} = 1 + \cos 2\theta \tag{18}$$

$$C_{\mathrm{II}} = 1 - \cos 2\theta \tag{19}$$

$$C_{\mathrm{III}} = C_{\mathrm{IV}} = \sin 2\theta \tag{20}$$

These values are determined as

$$C_{\mathrm{I}} = 1.4,\ C_{\mathrm{II}} = 0.6\ C_{\mathrm{III}} = C_{\mathrm{IV}} = 0.9 \tag{21}$$

The ratios of the valence bond configurations were 5 (**I**) : 1 (**II**) : 2 (**III** = **IV**) under the drastic approximation. The antiferromagnetically coupled singlet state (**V**) in Fig. 3 is expressed by the superposition of the four valence bond structures **I–IV**. However, the broken symmetry molecular orbitals partly involve the contribution from π_{v}* orbital as illustrated in Fig. 4. This implies that much more valence bond configurations are required to express the spin projected broken symmetry state, quantitatively. Judging from the charge and spin densities

on the Cu_2O_2 core, the copper ion lies in the intermediate oxidation (IO) state (I < IO < II), while dioxygen in turn exists in the intermediate reduction (IR) state (O_2^{1-} < O_2^{m-} < O_2^{2-}; 1 < m < 2) as shown in **V** of Fig. 3. The intermediate valence structure **V** expresses the coupling between Cu(IO) and O_2(IR) anion.

In the models **1**–**4**, the total charge densities on the Cu sites (Cu1 and Cu2) estimated with the X-ray structures were 2.16, 2.03, 2.23, and 1.76, respectively, showing that the back charge transfer from the peroxide to the Cu(II) sites in **4** is much stronger than those in **1**–**3**. This tendency is attributable to the conversion from peroxide to oxygen molecule due to the distorted Cu_2O_2 core, which causes the strong mixing of the character of triplet oxygen molecule to the electronic structure of the Cu_2O_2 core. After geometry optimizations of **1**–**4**, the charge densities on the Cu sites reduced, namely the oxidation number of the Cu ions become close to monovalent cation. It indicates the decrease of the magnetic couplings between the Cu ions as shown above.

6. Natural orbitals and chemical indices

6.1 Natural orbitals

The orbital correlation diagram is exhibited in Fig. 4. Fig. 5 illustrates the SONOs of **1**–**4** in the LS state. The bonding symmetric (S) d_{xy}–d_{xy} orbital of the dicopper site interacts with S-type orbitals (σ^*, π_v^*, etc) of peroxide in SONO–1, while SONO+1 consists of the antisymmetric (A) d_{xy}+d_{xy} orbital and the π_h^* one. The π_h^* orbital is stabilized by the symmetry-allowed orbital interactions to afford HOMO as shown in Fig. 4. The SONOs delocalize on the whole Cu_2O_2 core. The delocalized orbital on the *xy*-plane can be attributable to the antiferromagnetic superexchange interactions between the Cu(II) ions via dioxygen. The SONO–1 of **1** was composed of the d_{xy}–d_{xy} and σ^* orbitals because of the planar Cu_2O_2 core structures. On the other hand, that of **4** consisted of the d_{xy}–d_{xy} and π^* orbitals because the butterfly core structure allows the d orbitals to interact with π^* orbitals. In **2** and **3**, both the σ^* and π^* orbitals of peroxide was involved in the formation of the SONO–1. These results indicate that the architecture of the Cu_2O_2 core strongly influences the d-p orbital interaction, attributing to the magnetic couplings and the chemical bond characters.

6.2 Occupation numbers and chemical indices

The natural orbital analysis clearly demonstrates that the Cu_2O_2 bonds exhibit intermediate bonding. Chemical indices such as effective bond order should be a useful index for the investigation of bond character (Isobe et al., 2003; Takano et al., 2008; Takano and Yamaguchi, 2007; Yamaguchi, 1990). Using the occupation numbers of SONOs (Table 4), these indices for **1**–**4** can be estimated with Eqs. (7), (10), (11), and (12).

The b values for **1**–**4** are summarized in Table 5. The b_{SOMO} values indicate that the Cu sites intermediately interact with each other through the binding dioxygen. The Cu_2O_2 bond is not a closed-shell type molecular orbital configuration (b_{SOMO} = 1.0), but an open shell configuration, where electrons partially occupy the antibonding SONO+1. This open-shell molecular orbital configuration ensures the strong antiferromagnetic superexchange interactions. The b_{HOMO} values for **1**–**4** were 0.997, showing the very weak spin polarization effect. The b_{SOMO} values increases as **4** << **3** < **1** < **2**, indicating the same tendency of the $|J_{ab}|$ values. Judging from the charge densities and the b_{SOMO} values, **4** estimates much smaller superexchange interaction between Cu(II) ions via peroxide than **1**–**3**, showing the smaller absolute value of J_{ab}. On the other hand, the b_{HOMO} values in models **1**–**4** are close to each

other, indicating that the spin polarization effects are insensitive to the ligand coordination. The natural orbital analysis clearly demonstrates that the antiferromagnetic couplings of these Cu_2O_2 system are dominated by the superexchange interaction and that the Cu(II) ions and the peroxide ion show an intermediate orbital interaction ($0 < b_{SOMO} < 1.0$).

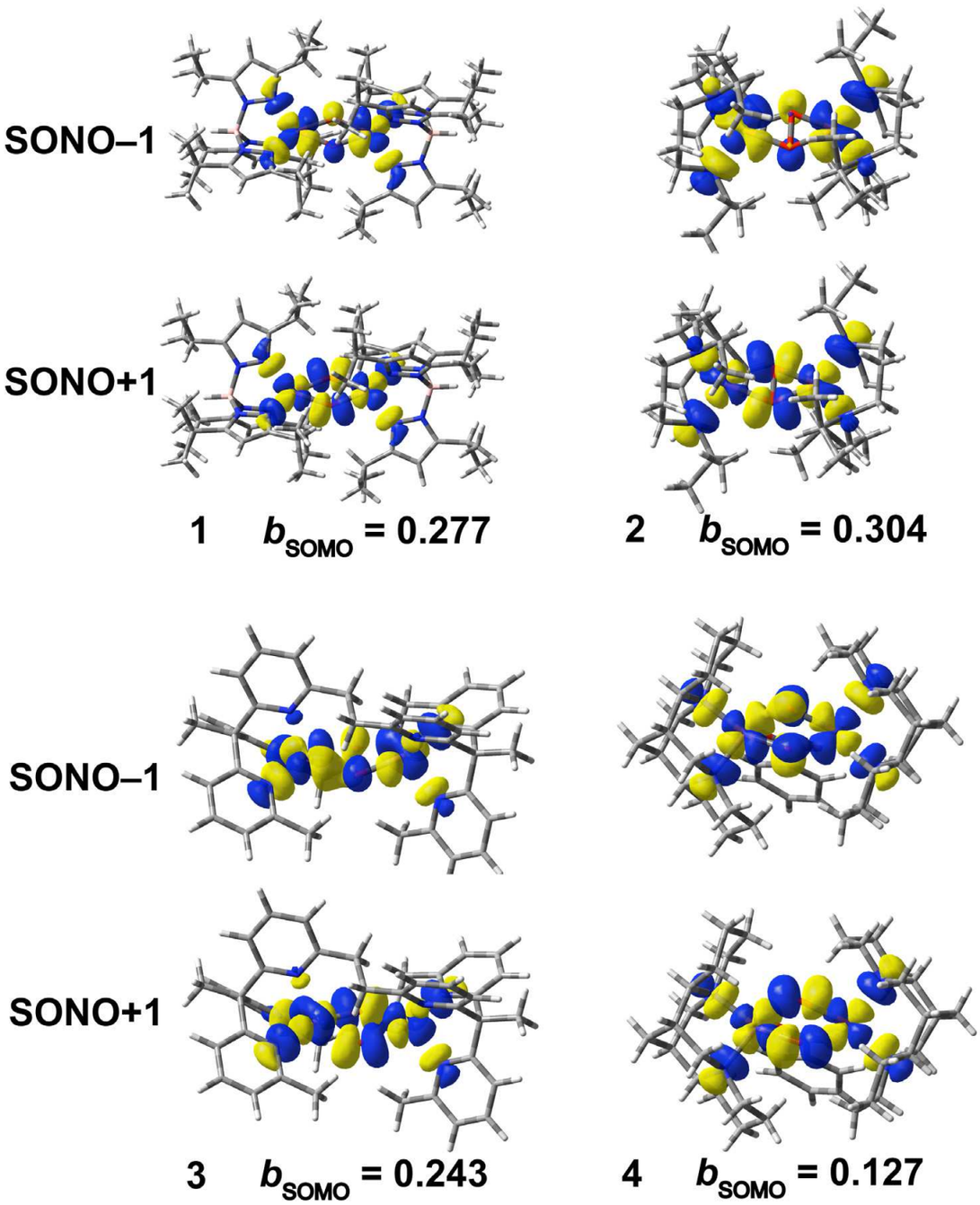

Fig. 5. Singly occupied bonding (SONO–1) and antibonding (SONO+1) natural orbitals (SONOs) obtained from UBHandHLYP calculations in the LS state with the X-ray crystallographic structures of **1–4**.

Model		HOMO	SOMO–1	SOMO+1	LUMO
1	X-ray	1.997	1.277	0.723	0.003
	Opt[a]	1.997	1.236	0.764	0.003
2	X-ray	1.997	1.304	0.696	0.003
	Opt[a]	1.997	1.253	0.747	0.003
3	X-ray	1.997	1.243	0.757	0.003
	Opt[a]	1.997	1.222	0.778	0.003
4	X-ray	1.997	1.127	0.873	0.003
	Opt[a]	1.998	1.091	0.909	0.002

[a] Geometrical parameters were fully optimized.

Table 4. Occupation Numbers of HOMO and SOMOs (SONOs) of **1–4** by UBHandHLYP in the LS State.

Model		b_{HOMO}	b_{SOMO}
1	X-ray	0.997	0.277
	Opt[a]	0.997	0.236
2	X-ray	0.997	0.304
	Opt[a]	0.997	0.253
3	X-ray	0.997	0.243
	Opt[a]	0.997	0.222
4	X-ray	0.997	0.127
	Opt[a]	0.998	0.091

[a] Geometrical parameters were fully optimized.

Table 5. Effective bond orders of HOMOs and SOMOs (SONOs) of **1–4** by UBHandHLYP in the LS State.

The information entropy (I), unpaired electron density (U), and diradical character (Y) are also useful indices for the investigation of the character of the chemical bond (Soda et al., 2000). Using the occupation numbers of the SONOs, the indices were estimated with Eqs. (10)–(12). In Table 6, the I values express the loss of the covalency of the chemical bonds. The U values are equivalent to the deviation from exact singlet value $^{LS}\langle \mathbf{S}^2 \rangle = 0$ for the broken-symmetry solution. The Y values, which characterize the double excitation of electrons occupying the bonding NOs, indicate how much the unoccupied electrons can localize on the spin sites. They can be regarded as useful indices to diagnose the bond nature and measures of the strength of orbital interactions. Previously, we investigated the nature of the chemical bonds of organic systems, showing that intermolecular radical character of organic radicals, phenalenyl radical dimeric pair, were represented as 0.65 of the I value, 0.838 of the U value, and 0.30 of the Y value (Takano et al., 2002b, c). Comparing to the organic system, we found that the biomimetic complexes, **1–4**, show strong radical character, that is, rather weak orbital interactions; however, the weak bond character is sufficient for the cooperative intramolecular (through-bond) charge transport for the oxygen trapping, namely the dioxygen binding in the biomimetic complexes, **1–4**. The estimated effective bond orders and information entropies exhibit similar behavior responsible for the bond formation via electron delocalization. On the other hand, the evaluted unpaired electron densities are responsible for the electron correlation effects, and therefore they are about 1.0 for all the complexes, indicating an important role of the electron correlation effect. The electron

delocalization and electron correlations are competitive in the copper–oxygen systems. This is the reason why we must use UBHandHLYP instead of UB3LYP and UBLYP as discussed in detail in our previous paper (Takano et al., 2001; Takano and Yamaguchi, 2007). The optimized structure provided the larger chemical indices for **1–4** than the X-ray structure due to the relaxation of the Cu_2O_2 core. It indicates that crystal environment strengthens the orbital interactions of the dicopper core of the biomimetic complexes, **1–4**. The evaluated information entropies, unpaired electron densities, and diradical characters show the following tendency: **4** >> **3** > **1** > **2**, qualitatively corresponds to the order of the magnetic coupling: J_{ab}(**4**) >> J_{ab}(**3**) > J_{ab}(**1**) > J_{ab}(**2**).

Model		I_n	U	Y
1	X-ray	0.775	0.923	0.485
	Opt[a]	0.811	0.944	0.553
2	X-ray	0.75	0.908	0.443
	Opt[a]	0.796	0.936	0.524
3	X-ray	0.805	0.941	0.541
	Opt[a]	0.823	0.951	0.577
4	X-ray	0.903	0.984	0.75
	Opt[a]	0.931	0.992	0.819

[a] Geometrical parameters were fully optimized.

Table 6. Information entropies (I), unpaired electron densities (U), and diradical characters (Y) of SOMOs (SONOs) of **1–4** by UBHandHLYP in the LS State.

7. Concluding remarks

The magnetic couplings and the nature of the chemical bonds of the $Cu_2(\mu\text{-}\eta^2\text{:}\eta^2\text{-}O_2)$ core of the biomimetic models **1–4** were investigated by hybrid DFT calculations such as UBHandHLYP calculations.

We estimated the magnetic coupling constants and examined the electronic structures for **1–4** from the viewpoint of the shape and symmetry of the natural orbitals and chemical indices. Analysis of natural orbitals and effective bond orders provide us useful insights that the antiferromagnetic couplings of the Cu_2O_2 systems are dominated by the superexchange interaction, that Cu(II) ions and peroxide show an intermediate orbital interaction ($0 < b < 1.0$), and that the distortion of the Cu_2O_2 core from a planar structure to a butterfly structure and elongation of the Cu–O bonds cause the reduction of orbital interactions between the symmetric d_{xy}–d_{xy} orbital of the dicopper site and the π_v^* orbital of O_2 and between the antisymmetric d_{xy}+d_{xy} orbital and the π_h^* orbital, weakening the magnetic coupling between the Cu sites via $\mu\text{-}\eta^2\text{:}\eta^2$-peroxide. The information entropy, unpaired electron density, and diradical character exhibited the useful information about the chemical bonds in the dicopper core of biomimetic complexes, **1–4**. Especially, the evaluted unpaired electron densities indicates the reason why we must use UBHandHLYP instead of UB3LYP and UBLYP. Thus, natural orbitals and chemical indices such as effective bond order, information entropy, unpaired electron density, and diradical character are useful for elucidation of the nature of chemical bonds based on the broken symmetry DFT calculation.

8. References

Allen, F.H. (2002). The Cambridge Structural Database: a quarter of a million crystal structures and rising. Acta Crystallogr Sect B-Struct Sci *58*, 380-388.

Aullón, G., Gorun, S.M., & Alvarez, S. (2006). Effects of tris(pyrazolyl)borato ligand substituents on dioxygen activation and stabilization by copper compounds. Inorganic Chemistry *45*, 3594-3601.

Becke, A.D. (1988). Density-functional exchange-energy approximation with correct asymptotic behavior. Phys Rev A *38*, 3098.

Becke, A.D. (1993). Density-functional thermochemistry. III. The role of exact exchange. The Journal of Chemical Physics *98*, 5648-5652.

Benson, D.E., Haddy, A.E., & Hellinga, H.W. (2002). Converting a maltose receptor into a nascent binuclear copper oxygenase by computational design. Biochemistry *41*, 3262-3269.

Cahoy, J., Holland, P.L., & Tolman, W.B. (1999). Experimental studies of the interconversion of μ-η²:η²-peroxo- and bis(⌠-oxo)dicopper complexes. Inorganic Chemistry *38*, 2161-2168.

Cooksey, C.J., Garratt, P.J., Land, E.J., Pavel, S., Ramsden, C.A., Riley, P.A., & Smit, N.P.M. (1997). Evidence of the indirect formation of the catecholic intermediate substrate responsible for the autoactivation kinetics of tyrosinase. Journal of Biological Chemistry *272*, 26226-26235.

Cramer, C.J., Kinsinger, C.R., & Pak, Y. (2003). Mechanism of intramolecular C-H bond activation in $[(LCu)_2(⌠\text{-}O)_2]^{2+}$ (L = 1,4,7-trialkyl-1,4,7-triazacyclononane): Quantum mechanical/molecular mechanical modeling. Journal of Molecular Structure: THEOCHEM *632*, 111-120.

Cramer, C.J., & Pak, Y. (2001). Transition state for intramolecular C-H bond cleavage in $[(LCu)_2(\mu\text{-}O)_2]^{2+}$ (L = 1,4,7-tribenzyl-1,4,7-triazacyclononane). Theoretical Chemistry Accounts *105*, 477-480.

Cuff, M.E., Miller, K.I., Van Holde, K.E., & Hendrickson, W.A. (1998). Crystal structure of a functional unit from Octopus hemocyanin. Journal of Molecular Biology *278*, 855-870.

Frisch, M.J., Trucks, G.W., Schlegel, H.B., Scuseria, G.E., Robb, M.A., Cheeseman, J.R., Montgomery, J.A., Vreven, T., Kudin, K.N., Burant, J.C., *et al.* (2003). Gaussian 03, Revision C.02.

Funahashi, Y., Nishikawa, T., Wasada-Tsutsui, Y., Kajita, Y., Yamaguchi, S., Arii, H., Ozawa, T., Jitsukawa, K., Tosha, T., Hirota, S., *et al.* (2008). Formation of a bridged butterfly-type μ-η²:η²-peroxo dicopper core structure with a carboxylate group. Journal of the American Chemical Society *130*, 16444-16445.

Gresh, N., Policar, C., & Giessner-Prettre, C. (2002). Modeling copper(I) complexes: SIBFA molecular mechanics versus ab initio energetics and geometrical arrangements. J Phys Chem A *106*, 5660-5670.

Hariharan, P.C., & Pople, J.A. (1973). The influence of polarization functions on molecular orbital hydrogenation energies. Theor Chim Acta *28*, 213-222.

Hay, P.J. (1977). Gaussian basis sets for molecular calculations. The representation of 3d orbitals in transition-metal atoms. The Journal of Chemical Physics *66*, 4377-4384.

Hehre, W.J., Ditchfield, R., & Pople, J.A. (1972). Self-Consistent Molecular Orbital Methods. XII. Further Extensions of Gaussian-Type Basis Sets for Use in Molecular Orbital Studies of Organic Molecules. The Journal of Chemical Physics *56*, 2257-2261.

Holm, R.H., Kennepohl, P., & Solomon, E.I. (1996). Structural and Functional Aspects of Metal Sites in Biology. Chemical Reviews *96*, 2239-2314.

Hu, Z., George, G.N., & Gorun, S.M. (2001). Flourine encapsulation and stabilization of biologically relevant low-valence copper-oxo cores. Inorganic Chemistry *40*, 4812-4813.

Isobe, H., Takano, Y., Kitagawa, Y., Kawakami, T., Yamanaka, S., Yamaguchi, K., & Houk, K.N. (2002). Extended Hartree-Fock (EHF) theory of chemical reactions VI: hybrid DFT and post-Hartree-Fock approaches for concerted and non-concerted transition structures of the Diels-Alder reaction. Molecular Physics *100*, 717-727.

Isobe, H., Takano, Y., Kitagawa, Y., Kawakami, T., Yamanaka, S., Yamaguchi, K., & Houk, K.N. (2003). Systematic comparisons between broken symmetry and symmetry-adapted approaches to transition states by chemical indices: A case study of the Diels-Alder reactions. J Phys Chem A *107*, 682-694.

Karlin, K.D., & Tyeklár, Z. (1993). Bioinorganic Chemistry of Copper (New York, Chamman & Hall).

Kitagawa, Y., Saito, T., Ito, M., Shoji, M., Koizumi, K., Yamanaka, S., Kawakami, T., Okumura, M., & Yamaguchi, K. (2007). Approximately spin-projected geometry optimization method and its application to di-chromium systems. Chemical Physics Letters *442*, 445-450.

Kitajima, N., Fujisawa, K., Fujimoto, C., Moro-oka, Y., Hashimoto, S., Kitagawa, T., Toriumi, K., Tatsumi, K., & Nakamura, A. (1992). A new model for dioxygen binding in hemocyanin. Synthesis, characterization, and molecular structure of the μ-η^2:η^2 peroxo dinuclear copper(II) complexes, $[Cu(HB(3,5\text{-}R_2pz)_3)]_2(O_2)$ (R = *i*-Pr and Ph). Journal of the American Chemical Society *114*, 1277-1291.

Kitajima, N., Fujisawa, K., Moro-oka, Y., & Toriumi, K. (1989). μ-η^2:η^2-Peroxo binuclear copper complex, $[Cu(HB(3,5\text{-}iPr_2pz)_3)]_2(O_2)$. Journal of the American Chemical Society *111*, 8975-8976.

Kitajima, N., & Moro-oka, Y. (1994). Copper-dioxygen complexes. Inorganic and bioinorganic perspectives. Chemical Reviews *94*, 737-757.

Kodera, M., Kajita, Y., Tachi, Y., Katayama, K., Kano, K., Hirota, S., Fujinami, S., & Suzuki, M. (2004). Synthesis, Structure, and Greatly Improved Reversible O_2 Binding in a Structurally Modulated μ-η^2:η^2-Peroxodicopper(II) Complex with Room-Temperature Stability. Angewandte Chemie - International Edition *43*, 334-337.

Kodera, M., Katayama, K., Tachi, Y., Kano, K., Hirota, S., Fujinami, S., & Suzuki, M. (1999). Crystal structure and reversible O_2-binding of a room temperature stable μ-η^2:η^2-peroxodicopper(II) complex of a sterically hindered hexapyridine dinucleating ligand. Journal of the American Chemical Society *121*, 11006-11007.

Lam, B.M.T., Halfen, J.A., Young Jr, V.G., Hagadorn, J.R., Holland, P.L., Lledós, A., Cucurull-Sánchez, L., Novoa, J.J., Alvarez, S., & Tolman, W.B. (2000). Ligand macrocycle structural effects on copper-dioxygen reactivity. Inorganic Chemistry *39*, 4059-4072.

Lee, C., Yang, W., & Parr, R.G. (1988). Development of the Colle-Salvetti correlation-energy formula into a functional of the electron density. Physical Review B *37*, 785.

Maseras, F., & Morokuma, K. (1995). IMOMM: A new integrated ab initio + molecular mechanics geometry optimization scheme of equilibrium structures and transition states. J Comput Chem *16*, 1170-1179.

Mitani, M., Mori, H., Takano, Y., Yamaki, D., Yoshioka, Y., & Yamaguchi, K. (2000a). Density functional study of intramolecular ferromagnetic interaction through *m*-phenylene coupling unit (I): UBLYP, UB3LYP, and UHF calculations. Journal of Chemical Physics *113*, 4035-4051.

Mitani, M., Yamaki, D., Takano, Y., Kitagawa, Y., Yoshioka, Y., & Yamaguchi, K. (2000b). Density-functional study of intramolecular ferromagnetic interaction through *m*-phenylene coupling unit (II): Examination of functional dependence. Journal of Chemical Physics *113*, 10486-10504.

Onishi, T., Takano, Y., Kitagawa, Y., Kawakami, T., Yoshioka, Y., & Yamaguchi, K. (2001). Theoretical study of the magnetic interaction for M-O-M type metal oxides. Comparison of broken-symmetry approaches. Polyhedron *20*, 1177-1184.

Ramirez, J.C., Soriano, C., Esquivel, R.O., Sagar, R.P., Ho, M.H., & Smith, V.H. (1997). Jaynes information entropy of small molecules: Numerical evidence of the Collins conjecture. Phys Rev A *56*, 4477-4482.

Rappe, A.K., Casewit, C.J., Colwell, K.S., Goddard, W.A., & Skiff, W.M. (1992). UFF, a full periodic table force field for molecular mechanics and molecular dynamics simulations. Journal of the American Chemical Society *114*, 10024-10035.

Roos, B.O., Linse, P., Siegbahn, P.E.M., & Blomberg, M.R.A. (1982). A simple method for the evaluation of the 2nd-order perturbation energy from external double-excitations with a CASSCF reference wavefunction. Chem Phys *66*, 197-207.

Saito, T., Kataoka, Y., Nakanishi, Y., Matsui, T., Kitagawa, Y., Kawakami, T., Okumura, M., & Yamaguchi, K. (2010). Which hybrid GGA DFT is suitable for Cu_2O_2 systems if the spin contamination error is removed? Chem Phys *368*, 1-6.

Saito, T., Kitagawa, Y., Shoji, M., Nakanishi, Y., Ito, M., Kawakami, T., Okumura, M., & Yamaguchi, K. (2008). Theoretical studies on the structure and effective exchange integral (J_{ab}) of an active site in oxyhemocyanin (oxyHc) by using approximately spin-projected geometry optimization (AP-opt) method. Chemical Physics Letters *456*, 76-79.

Salem, L. (1982). Electrons in Chemical Reactions: First Principle (New York, Wiley).

Siegbahn, P.E.M. (2006). The performance of hybrid DFT for mechanisms involving transition metal complexes in enzymes. Journal of Biological Inorganic Chemistry *11*, 695-701.

Siegbahn, P.E.M., & Wirstam, M. (2001). Is the Bis-m-Oxo Cu2(III,III) state an intermediate in tyrosinase? Journal of the American Chemical Society *123*, 11819-11820.

Soda, T., Kitagawa, Y., Onishi, T., Takano, Y., Shigeta, Y., Nagao, H., Yoshioka, Y., & Yamaguchi, K. (2000). Ab initio computations of effective exchange integrals for H-H, H-He-H and Mn_2O_2 complex: comparison of broken-symmetry approaches. Chemical Physics Letters *319*, 223-230.

Solomon, E.I., Baldwin, M.J., & Lowery, M.D. (1992). Electronic structures of active sites in copper proteins: Contributions to reactivity. Chemical Reviews *92*, 521-542.

Staroverov, V.N., & Davidson, E.R. (2000). Transition regions in the cope rearrangement of 1,5-hexadiene and its cyano derivatives. Journal of the American Chemical Society *122*, 7377-7385.

Takano, Y., Isobe, H., & Yamaguchi, K. (2008). Theoretical studies on electronic structures and chemical indices of the active site of oxygenated and deoxygenated hemerythrin. Bulletin of the Chemical Society of Japan *81*, 91-102.

Takano, Y., Kitagawa, Y., Onishi, T., Yoshioka, Y., Yamaguchi, K., Koga, N., & Iwamura, H. (2002a). Theoretical studies of magnetic interactions in Mn(II)(hfac)$_2${di(4-pyridyl)phenylcarbene} and Cu(II)(hfac)$_2${di(4-pyridyl)phenylcarbene}. Journal of the American Chemical Society *124*, 450-461.

Takano, Y., Koizumi, K., & Nakamura, H. (2009). Theoretical studies of the magnetic couplings and the chemical indices of the biomimetic models of oxyhemocyanin and oxytyrosinase. Inorg Chim Acta *362*, 4578-4584.

Takano, Y., Kubo, S., Onishi, T., Isobe, H., Yoshioka, Y., & Yamaguchi, K. (2001). Theoretical studies on the magnetic interaction and reversible dioxygen binding of the active site in hemocyanin. Chemical Physics Letters *335*, 395-403.

Takano, Y., Soda, T., Kitagawa, Y., Onishi, T., Yoshioka, Y., & Yamaguchi, K. (2000). Theoretical study on magnetic interactions of Mn-pi conjugated system. Molecular Crystals and Liquid Crystals *342*, 291-296.

Takano, Y., Taniguchi, T., Isobe, H., Kubo, T., Morita, Y., Yamamoto, K., Nakasuji, K., Takui, T., & Yamaguchi, K. (2002b). Effective exchange integrals and chemical indices for a phenalenyl radical dimeric pair. Chemical Physics Letters *358*, 17-23.

Takano, Y., Taniguchi, T., Isobe, H., Kubo, T., Morita, Y., Yamamoto, K., Nakasuji, K., Takui, T., & Yamaguchi, K. (2002c). Hybrid density functional theory studies on the magnetic interactions and the weak covalent bonding for the phenalenyl radical dimeric pair. Journal of the American Chemical Society *124*, 11122-11130.

Takano, Y., & Yamaguchi, K. (2007). Hybrid density functional study of ligand coordination effects on the magnetic couplings and the Dioxygen binding of the models of hemocyanin. International Journal of Quantum Chemistry *107*, 3103-3119.

Takatsuka, K., Fueno, T., & Yamaguchi, K. (1978). Distribution of odd electrons in ground-state molecules. Theor Chim Acta *48*, 175-183.

Tatewaki, H., & Huzinaga, S. (1979). A systematic preparation of new contracted Gaussian type orbital set. I. Transition metal atoms from Sc to Zn. The Journal of Chemical Physics *71*, 4339-4348.

Trofimenko, S. (1999). Scorpionates: the coordination chemistry of polypyrazolborate ligands (London, Imperial College Press).

Vosko, S.H., Wilk, L., & Nusair, M. (1980). Accurate spin-dependent electron liquid correlation energies for local spin-density calculations-a critical analysis. Can J Phys *58*, 1200-1211.

Yamaguchi, K. (1990). In Self-Consistent Field Theory and Applications, R. Carbo, and M. Klobukowski, eds.

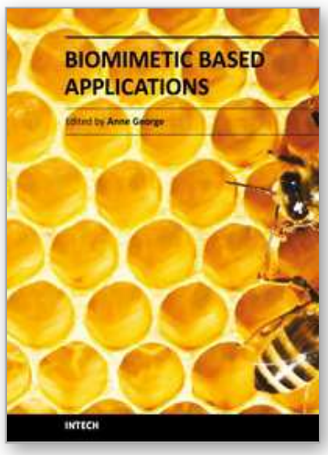

Biomimetic Based Applications

Edited by Prof. Marko Cavrak

ISBN 978-953-307-195-4
Hard cover, 572 pages
Publisher InTech
Published online 26, April, 2011
Published in print edition April, 2011

The interaction between cells, tissues and biomaterial surfaces are the highlights of the book "Biomimetic Based Applications". In this regard the effect of nanostructures and nanotopographies and their effect on the development of a new generation of biomaterials including advanced multifunctional scaffolds for tissue engineering are discussed. The 2 volumes contain articles that cover a wide spectrum of subject matter such as different aspects of the development of scaffolds and coatings with enhanced performance and bioactivity, including investigations of material surface-cell interactions.

How to reference

In order to correctly reference this scholarly work, feel free to copy and paste the following:

Yu Takano, Kizashi Yamaguchi and Haruki Nakamura (2011). Chemical Indices of the Biomimetic Models of Oxyhemocyanin and Oxytyrosinase, Biomimetic Based Applications, Prof. Marko Cavrak (Ed.), ISBN: 978-953-307-195-4, InTech, Available from: http://www.intechopen.com/books/biomimetic-based-applications/chemical-indices-of-the-biomimetic-models-of-oxyhemocyanin-and-oxytyrosinase

INTECH
open science | open minds

InTech Europe
University Campus STeP Ri
Slavka Krautzeka 83/A
51000 Rijeka, Croatia
Phone: +385 (51) 770 447
Fax: +385 (51) 686 166
www.intechopen.com

InTech China
Unit 405, Office Block, Hotel Equatorial Shanghai
No.65, Yan An Road (West), Shanghai, 200040, China
中国上海市延安西路65号上海国际贵都大饭店办公楼405单元
Phone: +86-21-62489820
Fax: +86-21-62489821

IntechOpen